First in Class, Potent, and Orally Bioavailable NADPH Oxidase Isoform 4 (Nox4) Inhibitors for the Treatment of Idiopathic Pulmonary Fibrosis

Benoît Laleu, Francesca Gaggini, Mike Orchard, Laetitia Fioraso-Cartier, Laurène Cagnon, Sophie Houngninou-Molango, Angelo Gradia, Guillaume Duboux, Cédric Merlot, Freddy Heitz, Cédric Szyndralewiez, and Patrick Page*

Genkyotex, S.A., 14 Chemin des Aulx, CH-1228 Plan-Les-Ouates, Switzerland

Received June 23, 2010

We describe the design, synthesis, and optimization of first-in-class series of inhibitors of NADPH oxidase isoform 4 (Nox4), an enzyme implicated in several pathologies, in particular idiopathic pulmonary fibrosis, a life-threatening and orphan disease. Initially, several moderately potent pyrazolopyridine dione derivatives were found during a high-throughput screening campaign. SAR investigation around the pyrazolopyridine dione core led to the discovery of several double-digit nanomolar inhibitors in cell free assays of reactive oxygen species (ROS) production, showing high potency on Nox4 and Nox1. The compounds have little affinity for Nox2 isoform and are selective for Nox4/1 isoforms. The specificity of these compounds was confirmed in an extensive in vitro pharmacological profile, as well as in a counterscreening assay for potential ROS scavenging. Concomitant benefits are good oral bioavailability and high plasma concentrations in vivo, allowing further clinical trials for the potential treatment of fibrotic diseases, cancers, and cardiovascular and metabolic diseases.

Introduction

There is compelling evidence indicating the production of low molecular weight second messengers, so-called reactive oxygen species (ROS[a]), as cell-signaling molecules and their implications in signal transduction.[1,2] The molecules involved in signaling include the three successive reduction products of molecular oxygen such as superoxide ($O_2^{\bullet-}$), hydrogen peroxide (H_2O_2), and hydroxyl radical ($HO^{\bullet}$), as well as reactive nitrogen species (RNS) such as NO, peroxynitrite, and peroxychloride.[3−5] Each of these species possesses chemical properties that potentially affect their signaling function. ROS and RNS act as signaling molecules and key regulators of cell function and are produced in specific compartments and tissues where they fine-tune the fragile intracellular redox cell-signaling balance.[6−10] Superoxide ($O_2^{\bullet-}$) production is the first chemical step of initiation of the oxidative stress cascade.[11]

Although ROS are produced by a variety of intracellular mechanisms, it is now well established that the predominant cellular sources of these molecules are a family of multisubunit enzymes known as the NADPH oxidases.[12,13] NADPH oxidase enzymes (Nox) are a six-transmembrane (6-TM) domain protein family that catalyze the reduction of molecular oxygen

(O_2) to superoxide ($O_2^{\bullet-}$), the primary product of Nox activation.[14] Nox2 (also known as gp91 phox) was the historically first identified NADPH oxidase (Nox) family member. Initially found in phagocytes, it plays a role in host defense by giving an outward burst of ROS.[15] In the late 1990s, Nox2 and its homologues were defined as a protein family of seven different isoforms including the phagocyte Nox2 isoform and Nox1, Nox3, Nox4, Nox5, Duox1, and Duox2, which were identified in non-phagocytes cells.[14,16] Although all seven Nox isoforms catalyze the reduction of molecular oxygen, they differ in their tissue distribution, subcellular localization, subunit requirements, domain structure, and the mechanism by which they are activated.[14] Today, it is becoming more recognized that the Nox enzyme protein family participates as an important, and in many cases predominant, source of ROS in a large variety of diseases.[17,18]

The NADPH oxidase isoform 4 (Nox4) has gained considerable and growing attention during the past years because of its potential key involvement in a variety of diseases, some of which have high unmet medical needs, such as idiopathic pulmonary fibrosis (IPF),[19] pulmonary arterial hypertension (PAH),[20,21] diabetic nephropathy (DN),[22] and complications such as diabetic cardiomyopathy[23] and neuropathy and retinopathy[24] or cancers[25] like metastatic renal cell carcinoma (RCC).[26,27]

Nox4 is constitutively active and requires a two-transmembrane (2-TM) protein counterpart called p22[phox] in its active form. In humans, Nox4 is most abundantly expressed in the kidney,[28,29] hence originally termed renal oxidase (renox),[30] as well as in the lung.[31,32] Nox4 is distributed in the renal vasculature, mesangial cells, podocytes, tubular cells as well as myofibroblasts and epithelial cells, the last two types of cells being known to play a key role in the pathogenesis of idiopathic pulmonary fibrosis (IPF).[33] In the lung, Nox4 regulates myofibroblast synthesis of fibronectin and contractile responses to

---

*To whom correspondence should be addressed. Phone: +41228801025. Fax: +41228801013. E-mail: patrick.page@genkyotex.com.

[a] Abbreviations: ADME, absorption, distribution, metabolism, excretion; ADMET, absorption, distribution, metabolism, excretion, toxicity; Cl, clearance; DIPEA, *N,N*-diisopropylethylamine; DPI, diphenyliodonium; Fu, fraction unbound; Fz, bioavailability; hERG, the human ether-a-go-go-related gene; HPLC, high performance liquid chromatography; hFLMC, human fetal lung mesenchymal cells; HTS, high throughput screening; IPF, idiopathic pulmonary fibrosis; NADPH, nicotinamide adenine dinucleotide phosphate; Nox, nicotinamide adenine dinucleotide phosphate oxidase; QH, liver blood flow; RNS, reactive nitrogen species; ROS, reactive oxygen species; rt, room temperature; SAR, structure−activity-relationship; TGF, transforming growth factor.
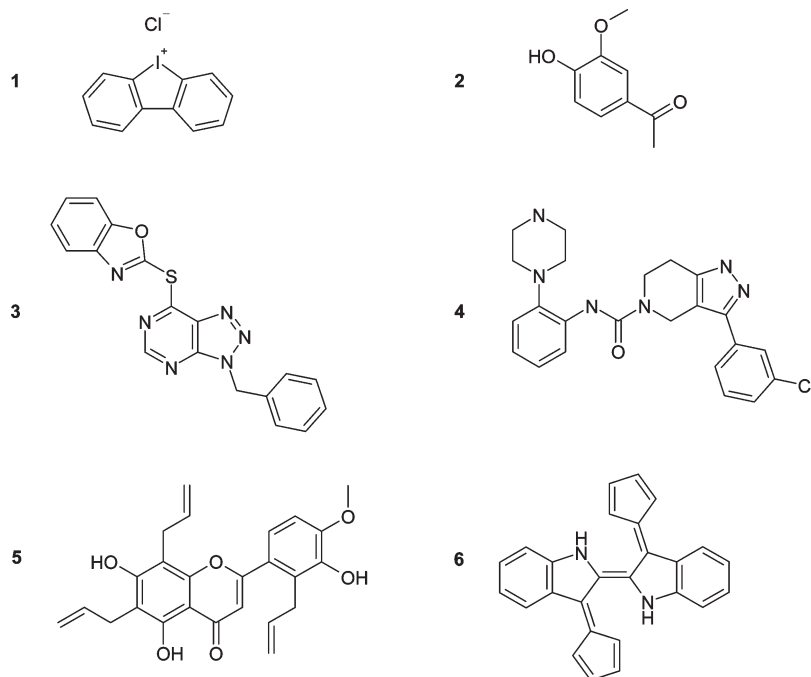
Figure 1. Structures of some known or claimed NADPH oxidases inhibitors: DPI (**1**), apocynin (**2**), VAS2870 (**3**), Shionigi compound (**4**), S17834 (**5**), and fulvene-5 (**6**).

the multifunctional cytokine, transforming growth factor-β1 (TGF-β1).[19] Nox4 is specifically induced by TGF-β1 in a time-dependent manner in hFLMCs and mediates H_2O_2 secretion by myofibroblasts.[19] The severity of idiopathic pulmonary fibrosis has been correlated with increased levels of H_2O_2 in the expired breath condensate (EBC) of IPF patients,[34] a biomarker directly linked to the NADPH oxidase 4 isoform. Nox4 mediates myofibroblasts differentiation and contractility and is induced in fibrotic lung injury in vivo.[19] Further data in animal models likewise point to a potential role for Nox4 modulation in idiopathic pulmonary fibrosis. RNAi-mediated inhibition of Nox4 protected against fibrotic lung injury. Furthermore, pharmacological unspecific inhibition of Nox flavoenzyme(s) activity by the irreversible inhibitor diphenyliodonium (**1**, Figure 1) dramatically diminished the deposition of collagen in a curative murine model of bleomycine-induced pulmonary fibrosis.[19]

Despite compelling evidence for the involvement of Nox enzymes in many signaling pathways and the great potential for the treatment of several pathologies, there is as of today no specific inhibitor of NADPH oxidases.[35] The above statement is very important and needs to be highlighted because a large number of studies investigating the role of Nox enzymes in pathological conditions rely on the use of molecules that are claimed to be specific. For instance, **1**, a toxic and nondruglike molecule, remains today the gold standard of Nox inhibitors although this molecule was demonstrated to be an irreversible and unselective inhibitor of several flavin-dependent enzymes such as nitric oxide synthase, xanthine oxidase, and others.[35] Also, **1** is an inhibitor of acetylcholinesterase and butyryl cholinesterase as well as of the internal Ca^{2+} pump,[36] which in addition to its intrinsic toxicity raises major concerns on the interpretation of studies performed with this molecule. Apocynin (**2**) is the claimed by some to be a Nox inhibitor.[37] However, this potentially reactive molecule is inactive in cell and membranes overexpressing Nox enzymes and decomposes in vivo in several entities which all contain catechol-like

antioxidant structural features.[38] Despite a recent publication that shows apocynin being not an inhibitor of Nox enzymes but an antioxidant,[39] it is still used as a reference compound although the resulting data may have to be carefully interpreted.

Furthermore, legions of molecules described in the literature wrongly named "Nox inhibitors" or "indirect Nox inhibitors" add to the general confusion.[40,41] These molecules such as **3** (VAS2870) are interfering with protein targets and signaling pathways that may affect Nox enzymes.[42] For instance, ARBs, ACEs, phosphodiesterase, eicosanoids, corticosteroids, MAP kinase, and protein kinase C inhibitors[42] such as Shionigi compound (**4**) and many others including potential antioxidant, catechol-like molecule **5** (S17834) or fluorescent dyes and/or unstable molecules like fulvene-5 (**6**) have all been claimed to be Nox inhibitors[43−46] without any data demonstrating inhibition of Nox enzymes in cell free assays or counterscreening assays to eliminate potential ROS-scavenging properties.[42−47] Today, there is urgency to identify truly specific Nox inhibitors in order to unravel the promises of this protein family. These molecules should meet key requirements such as lack of unspecific ROS scavenging or antioxidant ability, demonstrating off-targets selectivity, low adverse effects profile, and strong in vivo pharmacological activity in relevant diseases models.

Particularly, the validation of in vivo efficacy of druglike and selective Nox4 inhibitors is needed and will provide new insights on the role of Nox4 in idiopathic pulmonary fibrosis and chronic kidney diseases (CKD).
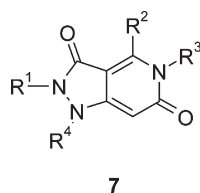
We set out to discover and develop first-in-class, potent, selective, and orally active Nox4 inhibitors as potential new therapeutic agents for the pharmacological management of IPF and CKD.

Results and Discussion

Primary Screening Results. A high-throughput screening (HTS) campaign using a cell free assay of ROS production on human Nox4 membranes was performed on 136 000

compounds. Several pyrazolopyridine diones (structure **7**, Figure 2) were moderately potent as confirmed in a concentration-response IC_{50} determination experiment (Table 1). The most potent compound was **12** with K_i(hNox4) = 373 nM. Incorporation of an acetyl group at R^4 position furnished derivative **18** almost equipotent to **12**, whereas the introduction of a benzyl group gave poorly active or inactive compounds. The very preliminary SAR obtained from this limited set of compounds suggested that the picolyl group at position R^3 could bring a beneficial effect although various groups gave some activity. Besides, phenyl substituents appeared to be preferred over benzothiazole groups at position R^1 and a triazolopyridazine resulted in a loss of activity.

Compound **12** was further evaluated in in vitro enzymatic assays and for early ADME properties (Table 2). This compound displayed a good Nox4/Nox2 selectivity (> 12-fold) and was also deprived of antioxidant properties based on a counterscreening assay for potential ROS scavenging (xanthine oxidase assay). Its in vitro early ADME profile showed a high intrinsic clearance in rat liver microsomes but a good permeability in the Caco-2 cell assay. The in vivo pharmacokinetic profile of **12** was therefore assessed in rat (Table 3). A high clearance was observed after intravenous dosing (Cl > liver blood flow, Q_H = 3.3 (L/kg)/h), which was in line with the in vitro data obtained for the microsomal metabolism. The short half-life of **12** might at least in part be related to high first-pass metabolism and translated in an apparent low oral bioavailability and poor exposure. The suspected strong first-pass metabolism was somehow corroborated by the really good bioavailability (F_Z = 87%) obtained after subcutaneous administration. Nevertheless, this compound had an acceptable volume of distribution (V_{ss} = 2.36 L/kg after iv injection).

Table 2. Pharmacological and Early in Vitro ADME Profile for Hit Compound **12**

parameter	
K_i (hNox4)[a]	373 ± 37 nM
K_i (hNox2)[b]	4720 ± 1280 nM
K_i (xanthine oxidase)[c]	>30000 nM
Cl (r-LM)[d]	97.1 (μL/min)/mg protein
Caco-2 (P_{app})[e]	79.2 × 10^{-6} cm/s

[a] Cell free assay of ROS production on Nox4 membranes. [b] Cell free assay of ROS production on Nox2 membranes (see Experimental Section). [c] In vitro enzymatic assay. [d] Microsome stability experiment. r-LM, rat liver microsomes (see Experimental Section). [e] Caco-2 cell permeability assay (see Experimental Section). P_{app}, permeability coefficient.


7

Figure 2. Structure of pyrazolopyridine dione core structure.

Table 1. Pyrazolopyridine Dione Derivatives from HTS Screening: Preliminary Exploration

Cpd.	Structure	K_i (nM)[a]	Cpd.	Structure	K_i (nM)[a]
8		4729 ± 536	**14**		5440 ± 11
9		1845 ± 368	**15**		1208 ± 53
10		9490 ± 236	**16**		878 ± 120
11		4222 ± 712	**17**		>30000
12		373 ± 37	**18**		409 ± 116
13		5232 ± 844	**19**		>30000

[a] Cell free assay of ROS production on human Nox4 membranes (see Experimental Section).

Table 3. In Vivo Pharmacokinetic Profile in Rat for Hit Compound **12**

route	dose (mg/kg)	AUC$_\infty$ (h·ng/mL)	F_Z (%)	C_{max} (ng/mL)	t_{max} (h)	$t_{1/2}$ (h)	Cl ((L/kg)/h)	V_{ss} (L/kg)
iv	1	196		271	0.08	0.40	5.11	2.36
sc	5	815	87	678	0.50	0.70		
os	10	417	22	575	0.25	1.20		

Scheme 1. Synthesis of Hit Compound **12** (General Procedure A)[a]
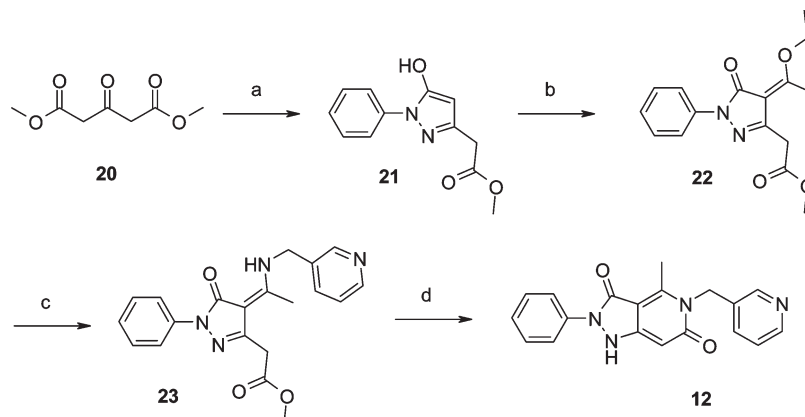
[a] Reagents and conditions: (a) phenylhydrazine, benzene, reflux, 80%; (b) Ac$_2$O, MeC(OEt)$_3$, reflux, 50%; (c) 3-aminomethylpyridine, toluene, reflux, 60%; (d) *i*-PrONa/*i*-PrOH, reflux, 58%.

On the basis of these data, compound **12** was considered as a suitable starting point for lead optimization. In the following chapters, we describe the SAR and the synthesis of pyrazolopyridine dione core structures.

Chemistry. The synthesis of pyrazolopyridine dione scaffold **7** was versatile and allowed the development of a quite extensive lead optimization program involving substitutions of the four diversity points of the scaffold (R^1, R^2, R^3, R^4, as illustrated in Figure 2).

The synthetic route of hit compound **12** consisted of a four-step procedure described in Scheme 1. In the first approach, the pyrazolone moiety **21** was built by condensation of commercially available dimethyl 1,3-acetonedicarboxylate **20** and phenylhydrazine[48] in benzene warmed to reflux. In presence of an excess of triethyl orthoacetate, pyrazolone **21** formed the enol ether **22**[49] which was easily converted into the corresponding enamine **23** in presence of 3-picolylamine in toluene heating at reflux.[48,50] The driving force of the reaction was the formation of final enamine which precipitated from the reaction mixture in good yield and high purity. Treatment of **23** with freshly prepared sodium isopropanolate[51,52] afforded the final product **12** in 14% overall yield. This procedure was applied to the synthesis of compounds **8**−**17** (Table 1).

The synthesis of final acetylated or alkylated analogues **18** and **19** (Table 1) and **41**−**48** (Table 4) was performed using different procedures. Acylation of **12** was achieved in 1 h with sodium acetate in acetic anhydride at 40 °C. Instead, DIPEA in DMF was used when a more hindered acyl chloride was selected (Scheme 2). Compounds **19** and **41**−**45** were obtained using standard protocol with several alkylating agents in the presence of triethylamine in THF (Scheme 3).
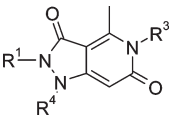
Alternative routes for the synthesis of pyrazolone derivative were also designed to overcome issues due to solvent toxicity. In the first instance, toluene replaced benzene and addition of DIPEA accelerated the condensation between the suitable hydrazine and the dimethyl 1,3-acetonedicarboxylate **20**. The second later improvement consisted of the use of methanol in the condensation step which was

performed at variable temperature (25−60 °C) depending on the intrinsic reactivity of the hydrazine. The final pyrazolone derivatives **28** were usually collected by precipitation in moderate to good yields. A key improvement concerned the second step: the use of a catalytic amount of glacial acetic acid rather than an excess of acetic anhydride resulted in much cleaner formation of the enol ether intermediates **29**. This modified route is outlined in Scheme 4. Following these procedures several libraries of this series of compounds (R^1 = Me) were synthesized (over 300 molecules), and the data for a representative set are shown in Table 4.

In order to investigate further the diversity point R^2, a modification of the synthetic strategy already illustrated was pursued and two different methods were developed: acyl chloride and 2-chloro-1,1,1-triethoxyethane pathways (Schemes 5 and 6, respectively). In the first case, condensation of commercially available acyl chlorides and pyrazolone **28** in 1,4-dioxane followed by Fries rearrangement was performed in the presence of calcium hydroxide under refluxing conditions (Scheme 5).[53,54] The obtained acylpyrazolone **33** was functionalized following the procedure already described: the enamine **34**, formed in acid conditions, was cyclized in milder conditions. The final product **35** was obtained after treatment with freshly prepared sodium methanolate solution at room temperature.

In the second approach, the reaction of pyrazolone **28** with an excess of 2-chloro-1,1,1-triethoxyethane under acid catalysis gave the possibility of exploring another route for lead optimization. Interestingly, and in contrast with the method described in Scheme 4, the expected enol ether **36** was never observed under UPLC conditions. Most probably in situ hydrolysis of enol ether **36** generated the α-chloroketone **37**, the only species detected by UPLC. Its intrinsic instability precluded any purification and characterization. The α-chloroketone **37** afforded the enamine **38** by reaction with a primary amine in acid conditions. In a subsequent step, the chlorine was displaced with a secondary amine in the presence of DIPEA under refluxing conditions. Final derivatives of type **40** were generated by cyclization of the

Table 4. SAR: R^4 Modification

Cpd.	R^1	R^3	R^4	K_i (nM)[a]
41	benzothiazol-2-yl	morpholin-4-yl	2-chlorobenzyl	>30000
42	benzothiazol-2-yl	tetrahydrofuran-2-ylmethyl	pyridin-2-ylmethyl	>30000
43	2-chlorophenyl	3-ethoxypropyl	pyridin-2-ylmethyl	>30000
44	phenyl	2-(indol-3-yl)ethyl	4-fluorobenzyl	>30000
45	phenyl	3-(2-oxopyrrolidin-1-yl)propyl	2-chlorobenzyl	>30000
46	phenyl	pyridin-3-ylmethyl	3-methoxyphenacyl	285
47	2-methylphenyl	pyridin-2-ylmethyl	acetyl	398
48	2-chlorophenyl	pyridin-2-ylmethyl	acetyl	240

[a] Cell free assay of ROS production on human Nox4 membranes.

intermediate compounds **39** with freshly prepared sodium methanolate solution.

Biological Activity. At first, the SAR around the R^4 part of the molecule was explored (Table 4). All tested N-alkylated derivatives were found inactive on Nox4, which confirmed the primary screening results. In contrast, acylated products were in the same range of potency as the hit **12**. Unfortunately, these compounds proved to be unstable (readily hydrolyzed at pH 6.5−8). These results discouraged us from further investigations on R^4-acylated compounds; therefore, lead optimization was focused on compounds bearing R^4 = H.

The influence of the R^1 substitution was investigated ($R^2 = R^3$ = Me). Table 5 shows the data for a representative set of compounds. **53** can be seen as a benchmark compound for the pyrazolopyridine dione core structure (K_i = 2175 nM on hNox4). Heterocyclic substitution at R^1 position gave disappointing results. On the other hand, meta-substituted phenyl substituent compounds were more active than the hit **12** with a large tolerance in functionalities: amide, nitrile,

halogens. A loss of potency was observed in the case of a *p*-benzyloxyphenyl substituted compound **55**, whereas ortho substitutions afforded the most potent compounds, for instance, compounds **54** and **49** ($K_i \approx 215$ nM) harboring a *p*-fluoro-*o*-chlorophenyl and an *o*-chlorophenyl group, respectively. Interestingly, the incorporation of an ortho substituent also allowed a dramatic decrease of the microsomal metabolism compared to meta-substituted derivatives (e.g., 49.3 (μL/min)/mg protein for **49** and 163.0 (μL/min)/mg protein for **57**).

After the *o*-chlorophenyl group was determined as the potential optimal substituent for R^1, the SAR at R^3 position was explored, keeping R^2 as a methyl group (Table 6). A wide variety of substituents were tolerated (benzylic, acetylenic, aliphatic groups with H-bond donor or acceptor moieties, etc.) as well as various functionalities (acyl hydrazine, alcohol, piperazine, morpholine, sulfonamide, and pyridine). Compounds **64** and **66** were found to present solubility issues. Among the tested compounds, **63** and **67** were the

most potent compounds with $K_i \approx 160$ nM. The potency of **61**, **67**, and **68** advocated for a beneficial effect of having a basic center at a three-atom distance from the core structure. Interestingly, α-substitution of the pyridine nitrogen atom of **67** with a morpholine resulted only in a slight decrease in activity.

The high potency demonstrated by **67** led us to investigate further the SAR and to look at the preferential combinations at R^1 with 2-picolyl as R^3 group (Table 7). Once again, several substituents were tolerated. Chloroquinoline was found as a possible heterocyclic substitution although the affinity for hNox4 remained unsatisfying ($K_i = 458$ nM for compound **80**). Benzylic and aliphatic groups were revealed to be potential alternatives to the phenyl susbtituents previously identified. Furthermore, incorporation of halogens into benzylic substituents brought beneficial effects: up to a

2-fold increase in potency compared to the unsusbtituted benzyl group (compounds **74**, **76**, and **77** vs **75**). Regarding phenyl derivative analogues of **67**, the *o*-tolyl group in compound **79** gave a product almost equipotent with **67** whereas the *p*-fluoro-*o*-chlorophenyl moiety engendered a weaker affinity ($K_i = 235$ nM for **78**). The length of the spacer connecting the pyrazolopyridine dione core to the aryl moiety was also studied, and no loss of activity was observed up to a three-atom chain (compounds **72** and **73**).

Finally, the SAR at R^2 position was explored while performing limited variations at R^1 and R^3 positions to fine-tune the best possible combinations (Table 8). The choice of R^1 group was restricted to *o*-chlorophenyl or *p*-fluoro-*o*-chlorophenyl with the exception of **82**. R^3 was chosen among a simple methyl group, alkyl ether chains, or heteroaryl derivatives such as picolyl groups. At first, the rigid structure of compound **91** showed an interesting affinity ($K_i = 128$ nM with $R^2 = o$-F-Ph). The spacer between the core structure and the aryl moiety was then investigated for the R^2 position. All compounds displayed substantial potencies ($K_i < 172$ nM) with a good tolerance of functionalities within the flexible chain introduced: aniline, amine, halogens, phenoxy, piperazine, and pyridine. Phenoxymethyl derivatives **82** and **90** were less potent ($K_i \approx 114-153$ nM) than the benzyloxymethyl analogues **88** and **89** ($K_i \approx 82-95$ nM). Replacement of the oxygen by a nitrogen atom in the spacer consolidated the SAR around R^2: more flexibility and/or additional basic centers ($K_i \approx 47$ nM for **87**) seemed to bring beneficial effects over the anilinomethyl spacer present in **84** and **86** ($K_i \approx 151-172$ nM). Incorporation of nitrogen heterocycles at R^2, such as pyrrolidine and piperazine, gave as well excellent results (compounds **83** and **85**). In summary, this optimization allowed the discovery of several double-digit nanomolar inhibitors (K_i down to 47 nM for **87**) with several possible combinations for R^1, R^2, and R^3 groups.

In order to select the best compounds for pharmacokinetic studies, the most active compounds were subjected to in vitro ADME profiling, in particular with respect to oxidative metabolism in human and rat liver microsomes and Caco-2 cellular permeation models. These results are combined in Table 9.
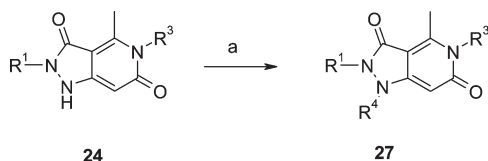
Most compounds showed moderate to low stability to microsomal metabolism in both species studied. Compounds **63**, **81**, **89**, and **90** exhibited a particularly high intrinsic
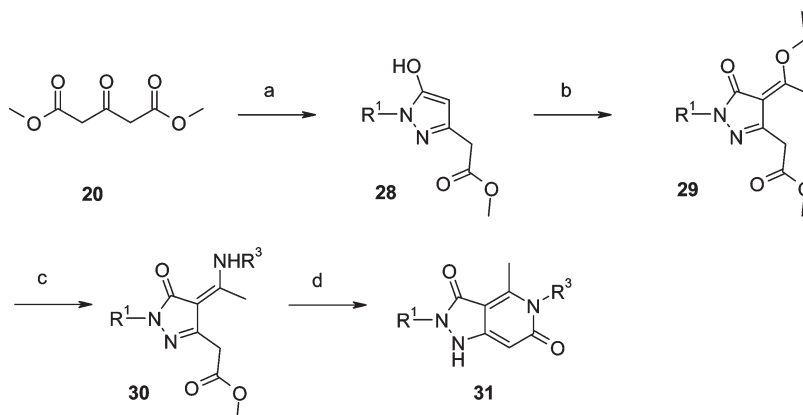
Scheme 2. Acylation Methods A and B[a]
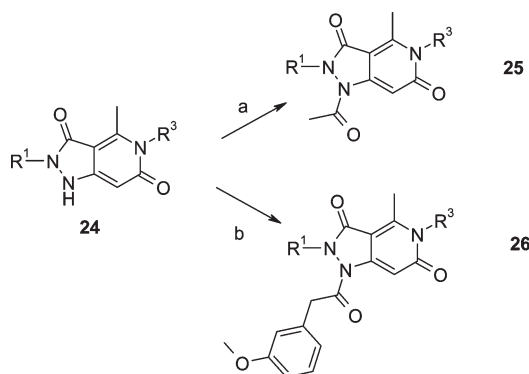
[a] Reagents and conditions: (a) Ac₂O/AcONa, 40 °C; (b) ArCH₂C-(O)Cl, DIPEA, DMF, 0 °C to rt.

Scheme 3. Alkylation method[a]

[a] Reagents and conditions: (a) R⁴X (X = Cl, Br), Et₃N, THF, reflux.

Scheme 4. Synthesis of Compounds of Type **31** ($R^2 = $ Me) (General Procedure B)[a]

[a] Reagents and conditions: (a) R¹NHNH₂, DIPEA, toluene, reflux; (b) glacial acetic acid (0.1 equiv), excess of MeC(OEt)₃, 60–70 °C; (c) R³NH₂, toluene, reflux; (d) *i*-PrONa/*i*-PrOH, reflux.

Scheme 5. Synthesis of Final Compounds of Type **35** (General Procedure C)[a]
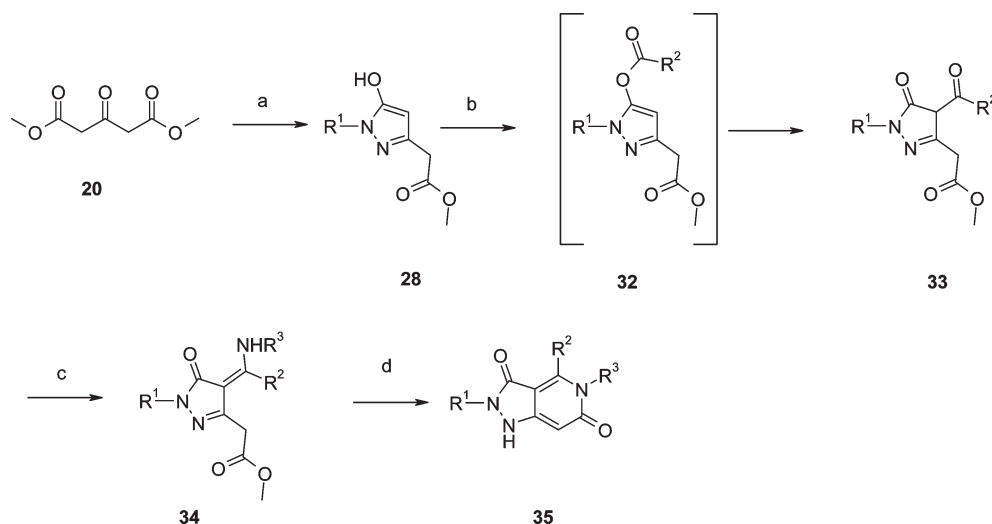
[a] Reagents and conditions: (a) R^1NHNH_2, MeOH, 25–60 °C; (b) $Ca(OH)_2$ (2 equiv), $R^2C(O)Cl$, 1,4-dioxane, reflux; (c) glacial acetic acid (0.1 equiv), R^3NH_2, toluene, 70 °C; (d) MeONa/MeOH, rt.

Scheme 6. Synthesis of Final Compounds of Type **40** (General Procedure D)[a]
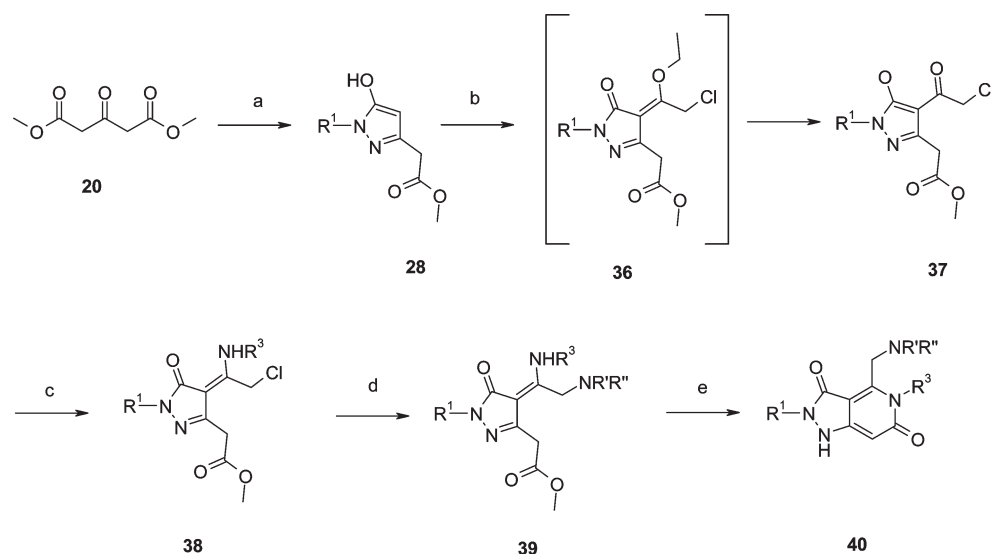
[a] Reagents and conditions: (a) R^1NHNH_2, MeOH, 25–60 °C; (b) glacial acetic acid (0.1 equiv), $ClCH_2C(OEt)_3$ (3 equiv), CH_3CN, 60–70 °C; (c) R^3NH_2, CH_3CN, rt; (d) $R'R''NH$, DIPEA, CH_3CN, reflux; (e) MeONa/MeOH, rt.

clearance in the rat liver microsomes (> 125 (μL/min)/mg protein). In the specific case of **90**, the metabolism was however moderate for human liver microsomes (49.3 (μL/min)/mg protein). On the other hand, **82**, **83**, and **88** had acceptable clearance values. The huge difference noted between the two structural analogues **88** and **89** could be explained by the higher lipophilicity of the latter compound making it more prone to phase I oxidative metabolism. Compound **67** displayed a slightly high clearance in the rat liver microsomes but a good stability to the human microsomes.

Concerning in vitro permeability, the P_{app} observed in Caco-2 experiments varied between 21.4 and 78.6×10^{-6} cm/s for most compounds. The very low values obtained for **82** and **87** can be explained in terms of log *D* properties (-0.35 and 1.15, respectively). These products were also characterized by a conspicuous efflux ratio that could be due to active transport (data not shown). Besides, compounds **83**, **84**,

and **87** have at least two basic centers that can be readily protonated, which might preclude them from easily crossing membranes.

Also, most molecules tested show no potential problem associated with CYP 450 inhibition (tested on five human isoforms CYP 1A2, 2C19, 2C9, 2D6, 3A4; data not shown). There were only a couple of exceptions: **84** showed multiple moderate to high inhibitions probably due to the presence of the easily accessible pyridine nitrogen in the para position ($IC_{50} \approx 4.1$ μM on CYP 2C9, $IC_{50} \approx 6.5$ μM on CYP 2C19, $IC_{50} \approx 1.1$ μM on CYP 3A4, and $IC_{50} \approx 3.6$ μM on CYP 2C8), and **81** inhibited primarily one isoform ($IC_{50} \approx 0.9$ μM on CYP 2C9, $IC_{50} \approx 13$ μM on CYP 2C19).

On the basis of the data gathered, five compounds were selected for in vivo pharmacokinetics studies in rat. The results are summarized in Table 10. As expected from in vitro data, **82** gave poor results with a very low oral bioavailability

Table 5. SAR: R^1 Modification

Cpd.	R^1	K_i (nM)[a]	Cpd.	R^1	K_i (nM)[a]
49		215 ± 22	54		213 ± 18
50		308 ± 59	55		3060
51		1947 ± 357	56		293 ± 45
52		1418 ± 435	57		340 ± 76
53	Me	2175	58		328 ± 37

[a] Cell free assay of ROS production on human Nox4 membranes.

and high in vivo clearance presumably because of its low permeability along with its physical properties ($P_{app} = 1.4 \times 10^{-6}$ cm/s with efflux and $\log D = -0.35$). Despite its low stability to rat liver microsomes but its extremely high plasma protein binding ($F_u = 0.0\%$ in 50% plasma protein), compound **90** showed suitable in vivo clearance and plasma concentrations and moderate oral bioavailability but low volume of distribution. Interestingly, the pharmacokinetic profile for both iv and per os routes strongly suggested the presence of enterohepatic circulation. This phenomenon is known to be potentially problematic because of its possible hepatotoxicity. **88** was a promising candidate with its high permeability ranking and reasonable stability to microsomal metabolism. A good exposure was indeed observed, but this compound displayed moderate bioavailability (29%) and a low volume of distribution ($V_{ss} = 0.35$ L/kg after iv dosing). Compound **83** proved to have an acceptable oral bioavailability (39%) with moderate plasma concentrations and volume of distribution. Finally, compound **67** displayed a good oral bioavailability associated with high plasma concentrations. After intravenous dosing, a half-life of 3.6 h was observed as well as acceptable distribution into tissues ($V_{ss} = 1.08$ L/kg). These in vivo data shed light on the beneficial effect of the *o*-chloro subtituent over the phenyl group at R^1 position with a dramatic improvement compared to the in vivo pharmacokinetic profile of the hit **12**. Compound **67** constitutes a good compromise between plasma protein

binding, microsomal metabolism, permeability, and physical properties ($\log D$, solubility, etc.).

The Nox4 specificity of **67** was confirmed vs Nox2 isoform (9-fold selectivity ratio) as well as in a counterscreening assay for potential ROS scavenging (Table 11). It is worth mentioning that this compound was proven to be a dual Nox4/Nox1 inhibitor ($K_i = 165$ and 160 nM, respectively). The most potent pyrazolopyridine diones on Nox4 also exhibited these key features (data not shown). The specificity of **67** was further confirmed in an extensive in vitro pharmacological profile (Table 12). Compound **67** had an excellent early in vitro ADMET profile (Table 13), and no potential problem was found regarding CYP 450 inhibition. This molecule was not mutagenic or genotoxic based on mini Ames and in vitro micronucleus tests. It also exhibited a low probability of generating QT prolongation based on lack of inhibition of hERG. Finally, the pyrazolopyridine dione **67** was demonstrated to have no toxicity up to 1000 mg/kg (per os) over a 2 week dose range finding in mice (data not shown), which confers a very large safety window to this compound.

Conclusion

We have identified a novel family of highly potent Nox4 inhibitors with dual activity on Nox1 and selectivity over the isoform Nox2. Exploration of the pyrazolopyridine dione class[58] focusing on R^1, R^2, R^3, and R^4 modifications afforded several compounds that showed good to excellent potency in

Table 6. SAR: R^3 Modification

Cpd.	R^3	K_i (nM)[a]	Cpd.	R^3	K_i (nM)[a]
59		520 ± 181	**64**		218 ± 138
60		565 ± 363	**65**		515 ± 142
61		235 ± 39	**66**		259 ± 19
62		428 ± 180	**67**		165 ± 5
63		158 ± 9	**68**		236 ± 12

[a] Cell free assay of ROS production on human Nox4 membranes.

our cell free assay of ROS production on human Nox4 membranes. Starting from our hit compound **12**, further improvement of the physical properties and pharmacological profiles led to the identification of the highly potent, orally bioavailable lead compound **67** (GKT136901). This compound demonstrated not only a straightforward synthetic procedure but also an excellent in vitro Nox isoforms specificity and pharmacological and safety profiles. Also, several molecules with K_i in the two digit nanomolar range on Nox4 and Nox1 were discovered. Those molecules proved to be highly potent in in vitro assays on human fibroblasts differentiation and epithelial cells apoptosis and epithelial-mesenchymal transition (EMT), as well as in preventive and curative murine models of bleomycin induced pulmonary fibrosis. The best pyrazolopyridine dione derivatives deserve further clinical trials for the treatment of idiopathic pulmonary fibrosis.

Experimental Section

Chemistry. Solvents and chemicals were reagent grade or better and were obtained from commercial sources. All experiments dealing with moisture sensitive compounds were conducted under nitrogen. Melting points were measured with a Büchi B-540 melting point apparatus and were uncorrected. NMR spectra were recorded on Bruker AMX 500, 400, and 300 MHz spectrometers. Chemical shifts were referenced with respect to the residual solvent signals (DMSO, 2.50 ppm; CHCl$_3$, 7.26 ppm). Data were reported as follows: chemical shift (δ), integration, multiplicity (s = singlet, bs = broad singlet, d = doublet, t = triplet, dd = doublet of doublets, ddd = doublet of doublet of doublets, dt = doublet of triplets, td = triplet of doublets, q = quadruplet, m = multiplet). Coupling constants (J) are in hertz. UPLC (ultra-performance liquid chromatography) data were obtained using a Waters Acquity SQ detector operating with positive or negative

electrospray. Analytical HPLC data were obtained using a Waters 2690 separation module (Alliance) equipped with a Zorbax Extend C-18 column (50 mm × 4.6 mm, 1.8 μm). Detection was conducted at 254 nm and full scan at 210−400 nm with a photodiode array detector. The mobile phase was a linear gradient with a flow rate of 0.8 mL/min using a 10:90 A/B to 100:0 A/B mixture over 4 min. Solvent A was 0.1% formic acid in water, and solvent B was 0.1% formic acid in acetonitrile. Silica flash and reverse phase chromatography were performed using an Armen apparatus Spot Flash equipped with silica SI60 15−40 μm and RP18 25−40 μm cartridges respectively. For TLC (thin layer chromatography) alumina sheets from Merck coated with silica gel 60 F$_{254}$ were used. All tested compounds possessed a purity of at least 95% estabilished by HPLC. When the purity of a particular compound was less than 95%, the percent of purity was specified at the end of its synthesis in the Experimental Section. Reported yields were not optimized, the emphasis being on purity of product rather than quantity.

General Procedure A. Synthesis of Hit Compound 12. Methyl (5-Hydroxy-1-phenyl-1*H*-pyrazol-3-yl)acetate (21). A stirred mixture of dimethyl 1,3-acetonedicarboxylate (10 mmol, 1.74 g) and phenylhydrazine (10 mmol, 1.08 g) in dry benzene (50 mL) was heated under reflux for 8 h. The solvent was removed in vacuo and the product was separated by recrystallization from *i*-PrOH (20 mL), yielding a white solid (80% yield) which was pure enough for the following step. Mp 140−141 °C (parent). ^{1}H NMR (400 MHz, DMSO-d_6) δ 11.10 (1H, bs), 7.78 (2H, d, J = 7.9 Hz), 7.35 (2H, t, J = 7.6 Hz), 7.12 (1H, t, J = 7.4 Hz), 5.43 (1H, s), 3.68 (3H, s), 3.49 (2H, s). LC−MS 233.4 (M + H)$^+$.

Methyl [(4*Z*)-4-(1-Ethoxyethylidene)-5-oxo-1-phenyl-4,5-dihydro-1*H*-pyrazol-3-yl]acetate (22). A mixture of the obtained pyrazolone **21** (1.85 g, 7.97 mmol), acetic anhydride (1.00 mL), and triethyl orthoacetate (4.50 mL) was heated under reflux for 1 h and left overnight at room temperature. The resulting precipitate was collected by filtration and washed with diethyl ether

Table 7. SAR: R[1] Modification

Cpd.	R[1]	K_i (nM)[a]	Cpd.	R[1]	K_i (nM)[a]
69	Me—*	387 ± 34	**75**		463 ± 127
70		313 ± 22	**76**		342 ± 4
71		445 ± 10	**77**		259 ± 4
72		334 ± 4	**78**		235 ± 55
73		326 ± 12	**79**		173
74		218	**80**		458

[a] Cell free assay of ROS production on human Nox4 membranes.

(10 mL) in order to obtain the crude product (1.20 g, 80% HPLC purity, yellow solid) in 50% yield. The product was used for the following step without further manipulation. ^{1}H NMR (400 MHz, CDCl₃) δ 7.97 (2H, d, $J = 8.0$ Hz), 7.37 (2H, t, $J = 7.6$ Hz), 7.16 (1H, t, $J = 7.2$ Hz), 4.31 (2H, q, $J = 6.9$ Hz), 3.76 (2H, s), 3.73 (3H, s), 2.78 (3H, s), 1.42 (3H, t, $J = 7.1$ Hz). LC−MS 303.4 (M + H)⁺.

Methyl [(4Z)-5-Oxo-1-phenyl-4-{1-[(pyridin-3-ylmethyl)amino]-ethylidene}-4,5-dihydro-1H-pyrazol-3-yl]acetate (23). A stirred mixture of compound **22** (1.20 g, 3.97 mmol) and 3-aminomethylpyridine (0.45 g, 4 mmol) was heated under reflux in toluene (20 mL) for 0.5 h and left overnight at room temperature. The resulting enamine **23** (0.87 g) was collected by filtration and washed with ethyl ether (20 mL), yielding a white solid (60% yield). ^{1}H NMR (400 MHz, CDCl₃) δ 12.17 (1H, bs), 8.63 (2H, bs), 7.97 (2H, d, $J = 8.0$ Hz), 7.70 (1H, d, $J = 7.7$ Hz), 7.38 (3H, m), 7.18 (1H, t, $J = 7.2$ Hz), 4.71 (2H, d, $J = 5.9$ Hz), 3.82 (2H, s), 3.71 (3H, s), 2.38 (3H, s). LC−MS 365.6 (M + H)⁺.

4-Methyl-2-phenyl-5-(pyridin-3-ylmethyl)-1H-pyrazolo[4,3-c]-pyridine-3,6(2H,5H)-dione (12). A stirred solution of compound **23** (0.87 g, 2.39 mmol) in anhydrous i-PrOH (10 mL) was treated with a freshly prepared solution of i-PrONa−i-PrOH, obtained by dissolving sodium (0.055 g, 2.39 mmol) in i-PrOH (50 mL) under nitrogen. The reaction mixture was heated under reflux for 9 h, then cooled and neutralized to pH 7 with 20% HCl aqueous solution. The precipitate formed was filtered off, washed with water (20 mL), and air-dried. Chromatographically pure

product was obtained as a beige solid (0.46 g, 58% yield). ^{1}H NMR (400 MHz, DMSO-d_6) δ 10.80 (1H, bs), 8.49 (2H, bs), 7.73 (2H, d, $J = 8.0$ Hz), 7.56 (1H, d, $J = 7.7$ Hz), 7.45 (2H, t, $J = 7.6$ Hz), 7.36 (1H, m), 7.18 (1H, t, $J = 7.5$ Hz), 5.82 (1H, s), 5.38 (2H, s), 2.77 (3H, s). LC−MS 333.4 (M + H)⁺.

General Procedure B for Compounds of Type 31. Step 1: Synthesis of Pyrazolone Intermediate of Type 28. Pyrazolone Method A. To a suspension of the appropriate hydrazine (10.16 mmol) in anhydrous toluene (50 mL) were added DIPEA (3.55 mL, 20.32 mmol) and dimethyl 1,3-acetonedicarboxylate (**20**) (1.77 g, 10.16 mmol). The resulting mixture was heated at reflux for 18 h before being concentrated in vacuo. The resulting brown oil was purified by flash chromatography over SiO₂ (CH₂Cl₂/MeOH, gradient).

Pyrazolone Method B. To the solution of the appropriate hydrazine (10.16 mmol) in MeOH (25 mL) was added dimethyl 1,3-acetonedicarboxylate (**20**) (1.77 g, 10.16 mmol). The resulting mixture was heated at 40−65 °C for 1 h. The solvent was removed by evaporation, and the residue was purified by flash chromatography over SiO₂ (CH₂Cl₂/MeOH, gradient).

Step 2: Synthesis of Enol Ether Derivatives of Type 29. A stirred mixture of compound from step 1 (3.75 mmol), glacial acetic acid (21 μL, 0.375 mmol), and an excess of triethyl orthoacetate (2.0 mL) was heated at 75 °C for 1 h. The resulting solution was concentrated in vacuo to afford a syrup that was washed with diethyl ether and then dried in vacuo. Because of its relative instability, no further purification was attempted.

Table 8. SAR: R^1, R^2, and R^3 Optimization

Cpd.	R^1	R^2	R^3	K_i (nM)[a]
81				165 ± 13
82				153 ± 26
83				114 ± 11
84				151 ± 19
85			Me	65 ± 2
86				172 ± 25
87				47 ± 4
88				95 ± 6
89			Me	82 ± 14
90			Me	114 ± 11
91			Me	128 ± 17

[a] Cell free assay of ROS production on human Nox4 membranes.

Step 3: Synthesis of Enamine Derivative of Type 30. A stirred mixture of compound from step 2 (3.75 mmol) and appropriate amine (3.75 mmol) in toluene (20 mL) was stirred at room temperature for 15 min. The solvent was removed in vacuo. The resulting residue was dissolved in a minimum of CH_2Cl_2 and precipitated with diethyl ether. The desired product was usually obtained as a precipitate in good to moderate yields.

Step 4: Cyclization. Compound from step 3 (3.57 mmol) was treated with an isopropanolic solution of i-PrONa, obtained by dissolving sodium (0.082 g, 3.57 mmol) in i-PrOH (35 mL). The reaction mixture was heated under reflux for 1 h, then cooled and neutralized to pH 7 by addition of 20% HCl aqueous solution. The organic solvent was removed in vacuo, and water was added before placing the flask in the fridge overnight. The

precipitate formed was filtered off, washed with diethyl ether, and dried in vacuo to afford the desired pure product.

Following the above-described general procedure B, using the appropriate hydrazines and primary amines, compounds **49**, **53**, **54**, **63**, **67**, **68**, **78**, **79** were obtained with 20−52% overall yields.

2-(2-Chlorophenyl)-4,5-dimethyl-1H-pyrazolo[4,3-c]pyridine-3,6(2H,5H)-dione (49). Isolated as a white solid. ^{1}H NMR (400 MHz, DMSO-d_6) δ 10.56 (1H, bs), 7.61−7.59 (1H, m), 7.52−7.49 (1H, m), 7.45−7.42 (1H, m), 5.62 (1H, s), 3.43 (3H, s), 2.74 (3H, s). LC−MS 290.5 (M + H)[+].

2,4,5-Trimethyl-1H-pyrazolo[4,3-c]pyridine-3,6(2H,5H)-dione (53). Isolated as a yellow solid (94% HPLC purity). ^{1}H NMR (400 MHz, DMSO-d_6) δ 5.48 (1H, s), 3.40 (3H, s), 3.16 (3H, s), 2.72 (3H, s). LC−MS 194.3 (M + H)[+].

2-(2-Chloro-4-fluorophenyl)-4,5-dimethyl-1H-pyrazolo[4,3-c]-pyridine-3,6(2H,5H)-dione (54). Isolated as a yellowish solid. ^{1}H NMR (400 MHz, DMSO-d_6) δ 10.56 (1H, bs), 7.64 (1H, dd, J = 8.8 Hz, J = 3.2 Hz), 7.58 (1H, dd, J = 8.8 Hz, J = 5.6 Hz), 7.34 (1H, td, J = 8.8 Hz, J = 3.2 Hz), 7.25−7.20 (2H, m), 5.63 (1H, s), 3.43 (3H, s), 2.74 (3H, s). LC−MS 308.7 (M + H)[+].

2-(2-Chlorophenyl)-4-methyl-5-(3-phenylprop-2-yn-1-yl)-1H-pyrazolo[4,3-c]pyridine-3,6(2H,5H)-dione (63). Isolated as a yellowish solid. ^{1}H NMR (400 MHz, DMSO-d_6) δ 10.81 (1H, bs), 7.63−7.61 (1H, m), 7.55−7.52 (1H, m), 7.37−7.33 (3H, m), 4.35 (3H, m), 5.68 (2H, s), 5.17 (2H, s), 2.95 (3H, s). LC−MS 390.8 (M + H)[+].

2-(2-Chlorophenyl)-4-methyl-5-(pyridin-2-ylmethyl)-1H-pyrazolo-[4,3-c]pyridine-3,6(2H,5H)-dione (67). Isolated as a pale yellow solid. Mp 210−212 °C (HCl salt, dec). ^{1}H NMR (500 MHz, DMSO-d_6) δ 10.74 (1H, bs), 8.48−8.46 (1H, m), 7.79 (1H, td, J = 7.6 Hz, J = 1.9 Hz), 7.67−7.64 (1H, m), 7.60−7.56 (1H, m), 7.50−7.47 (2H, m), 7.33−7.28 (2H, m), 5.66 (1H, s), 5.41 (1H, s), 2.78 (13H, s). LC−MS 367.1 (M + H)[+].

2-(2-Chlorophenyl)-4-methyl-5-[(6-morpholin-4-ylpyridin-2-yl)-methyl]-1H-pyrazolo[4,3-c]pyridine-3,6(2H,5H)-dione (68). Iso-

lated as a yellowish solid (92% purity by HPLC). ^{1}H NMR (400 MHz, DMSO-d_6) δ 7.63−7.60 (1H, m), 7.57−7.52 (2H, m), 7.48−7.36 (2H, m), 6.77 (1H, d, J = 8.8 Hz), 6.48 (1H, d, J = 7.2 Hz), 5.70 (1H, s), 5.27 (2H, s), 3.62 (2H, t, J = 5.2 Hz), 3.36 (2H, t, J = 5.2 Hz), 2.77 (3H, s). LC−MS 452.3 (M + H)[+].

2-(2-Chloro-4-fluorophenyl)-4-methyl-5-(pyridin-2-ylmethyl)-1H-pyrazolo[4,3-c]pyridine-3,6(2H,5H)-dione (78). Isolated as a yellow solid. ^{1}H NMR (400 MHz, DMSO-d_6) δ 8.54 (1H, d, J = 4.4 Hz), 7.94 (1H, td, J = 8.0 Hz, J = 2.0 Hz), 7.67−7.59 (2H, m), 7.45−7.40 (2H, m), 7.35 (1H, td, J = 8.0 Hz, J = 2.0 Hz), 5.67 (1H, s), 5.43 (2H, s), 2.77 (3H, s). LC−MS 385.0 (M + H)[+].

4-Methyl-2-(2-methylphenyl)-5-(pyridine-2-ylmethyl)-1H-pyra-zolo[4,3-c]pyridine-3,6(2H,5H)-dione (79). Isolated as a yellow solid. ^{1}H NMR (400 MHz, DMSO-d_6) δ 10.71 (1H, bs), 8.47 (2H, d, J = 3.2 Hz), 7.78 (1H, t, J = 6.0 Hz), 7.38−7.28 (6H, m), 5.66 (1H, s), 5.41 (2H, s), 2.79 (3H, s), 2.25 (3H, s). LC−MS 347.5 (M + H)[+].

General Procedure C for the Synthesis of Compounds of Type 35. Starting from the appropriate pyrazolone of type **28** whose synthesis has been already described (pyrazolone method B), the following molecules were generated.

Step 1: Synthesis of C-Acylated Pyrazolone 33. A stirred solution of the appropriate pyrazolone **28** (1.9 mmol) in anhydrous 1,4-dioxane (10 mL) was treated with Ca(OH)$_2$ (0.282 g, 3.8 mmol) and the suitable acyl chloride (1.9 mmol) under N$_2$. The mixture was heated at 70 °C, and the rearrangement was easily monitored by HPLC or TLC system because the acylated oxygen product was less polar than the desired product (1−3 h). The solvent was concentrated in vacuo, and the residue was partitioned between dichloromethane (50 mL) and a mixture of

Table 11. Activities of Lead Compound **67** on Flavoenzymes

parameter	
K_i (hNox4)[a]	165 ± 5 nM
K_i (hNox1)[b]	160 ± 10 nM
K_i (hNox2)[c]	1530 ± 90 nM
K_i (xanthine oxidase)[d]	>30000 nM

[a] Cell free assay of ROS production on Nox4 membranes. [b] Cell free assay of ROS production on Nox1 membranes. [c] Cell free assay of ROS production on Nox2 membranes. [d] In vitro enzymatic assay.

Table 9. In Vitro ADME Characterization for Selected Compounds

compd	Cl (h-LM),[a] (μL/min)/mg protein	Cl (r-LM),[b] (μL/min)/mg protein	Caco-2 (P_{app}),[c] (10^{−6} cm/s)	log D [d]
63		178.0		3.18
67	24.8	70.2	21.4	1.59
68		71.6		2.21
78	37.6	84.2	13.4	1.73
81	96.4	248.0	39.9	2.03
82	45.1	45.3	1.4	−0.35
83	45.4	62.3	7.3	1.61
84	76.3	78.0	4.6	3.23
85	57.9	121.0		2.22
87	24.8	74.1	0.5	1.15
88	32.4	49.5	78.6	1.55
89	212.0	210.0	62.6	2.77
90	49.3	125.0	35.5	2.39

[a] Microsome stability experiment. h-LM, human liver microsomes. [b] Microsome stability experiment. r-LM, rat liver microsomes. [c] Caco-2 cell permeability assay. P_{app}, permeability coefficient. [d] Calculated at pH 7.4.

Table 12. In Vitro Pharmacological Profile of Lead **67**

off target assay	inhibition at 10 μM (%)	off target assay	inhibition at 10 μM (%)
12-lipoxygenase (h)	2.0	p38 MAP kinase (h)	10.0
15-lipoxygenase	0	MEK1 (h)	0
AMPK (r)	0	myeloperoxidase (h)	0
ASK1 (h)	0	PKCα,β,δ (h)	0
Ca^{2+} channel	0	PI 3Kα,β,γ,δ	0
Cl^{−} channel	0	PTP1B (h)	0
Na^{+} channel	4.0	iNOS	0
K^{+} channel	0	eNOS (h)	6.0
MAO-B	0	ET$_A$ (h)	0

Table 10. In Vivo Pharmacokinetic Profile in Rats for Selected Compounds

compd	route	dose (mpk)	AUC_∞ (h·ng/mL)	F_Z (%)	C_{max} (ng/mL)	T_{max} (h)	$t_{1/2}$ (h)	Cl ((L/kg)/h)	V_{ss} (L/kg)
67	iv	5	10979		12126		3.63	0.47	1.08
	os	10	10937	54	3147	1.50			
82	iv	5	822		4637			6.52	2.95
	os	10	109	6	132	0.25	2.35	96.50	
83	iv	5	3130		6191		3.30	1.61	1.49
	os	10	2427	39	2834	0.33	1.13	4.39	
88	iv	5	15381		36754		3.14	0.33	0.35
	os	10	8933	29	6083	0.25	2.38	1.20	
90	iv	5	6528		30383		3.47	0.77	0.80
	os	10	3633	28	558	1.17	3.03	2.92	

Table 13. Early in Vitro ADMET Profile of **67**

parameter	
IC$_{50}$ (1A)^a	>25 μM
IC$_{50}$ (2C19)^a	>25 μM
IC$_{50}$ (2C9)^a	>25 μM
IC$_{50}$ (2D6)^a	>25 μM
IC$_{50}$ (3A4)^a	20.9 μM
Cl (h-LM)^b	24.8 (μL/min)/mg protein
Cl (r-LM)^c	70.2 (μL/min)/mg protein
Caco-2 (P_{app})^d	21.4 $\times$ 10^{-6} cm/s
F_u^{e}	20.5%
hERG^f	0% at 1 μM
mini AMES test^g	negative
in vitro micronucleus^h	negative

^{a} Inhibition of cytochrome P450 isoforms (see Experimental Section). ^{b} Microsome stability experiment. h-LM, human liver microsomes. ^{c} Microsome stability experiment. r-LM, rat liver microsomes. ^{d} Caco-2 cell permeability assay. P_{app}, permeability coefficient. ^{e} Plasma protein binding assay (in 50% plasma protein). ^{f} Conventional patch-clamp. ^{g} Performed at 100 μM. ^{h} Performed at 500 μM.

brine (10 mL) and 2 M HCl (1 mL, 2.00 mmol). The organic phase was separated, and the aqueous one was extracted with dichloromethane (50 mL) and then ethyl acetate (50 mL). The combined organic phases were dried over Na$_2$SO$_4$ and the solvent was evaporated to give the final product pure enough to be used for the following step without further purification.

Step 2: Synthesis of Enamine of Type 34. Compound from step 1 (1.9 mmol) was dissolved in toluene (20 mL), and the appropriate amine (1.9 mmol) and glacial acetic acid (0.12 mL, 2.09 mmol) were added at room temperature under N$_2$. The reaction mixture was stirred at 70 °C and monitored by LC−MS showing the disappearance of the starting material. The reaction mixture was evaporated until dryness. The residue was dissolved with a minimum amount of ethyl acetate (containing 0.1% triethylamine) and passed through a silica gel plug, eluting with ethyl acetate/ 0.1% triethylamine. Evaporation of the solvent gave the desired enamine which was used in the following step without further purification.

Step 3: Cyclization. The enamine from step 2 (1.4 mmol) was treated with a freshly prepared solution of MeONa in MeOH (2 M, 20 mL). The solution was stirred at room temperature until disappearance of the starting enamine (0.5−2 h). The reaction mixture was concentrated in vacuo to eliminate MeOH, and the crude was dissolved in ethyl acetate (80 mL) and extracted with water (3 × 30 mL). Then combined inorganic layers were acidified to pH 6, extracted with ethyl acetate (3 × 30 mL) and the combined organic layers dried over Na$_2$SO$_4$. The crude was purified by silica chromatography or reverse phase chromatography to afford the desired product.

Following the above-described general procedure C, using the appropriate hydrazines, acyl chloride, and primary amines, compounds **82**, **84**, and **88−90** were obtained with 15−30% overall yield.

4-[(4-Fluorophenoxy)methyl]-5-(2-methoxyethyl)-2-(2-morpholin-4-ylethyl)-1*H*-pyrazolo[4,3-*c*]pyridine-3,6(2*H*,5*H*)-dione (82). Isolated as red solid. Mp 48−49 °C (HCl salt). ^{1}H NMR (400 MHz, DMSO-*d*$_6$) δ 10.78 (1H, bs), 7.18−7.09 (4H, m), 5.91 (1H, s), 5.68 (2H, s), 4.35−4.25 (2H, m), 4.10−4.00 (2H, m), 3.98−3.90 (2H, m), 3.80−3.65 (2H, m), 3.60−3.40 (6H, m), 3.20 (3H, s), 3.15−3.05 (2H, m). LC−MS 447.3 (M + H)$^+$.

2-(2-Chlorophenyl)-4-{[methyl(phenyl)amino]methyl}-5-(pyridin-4-ylmethyl)-1*H*-pyrazolo[4,3-*c*]pyridine-3,6(2*H*,5*H*)-dione (84). Isolated as a yellow solid. ^{1}H NMR (400 MHz, DMSO-*d*$_6$) δ 11.26 (1H, bs), 8.55 (2H, d, *J* = 6.4 Hz), 7.70−7.63 (2H, m), 7.54−7.52 (2H, m), 7.26 (2H, d, *J* = 6.4 Hz), 7.04 (2H, t, *J* = 4.4 Hz), 6.70 (2H, t, *J* = 7.2 Hz), 6.50 (1H, d, *J* = 7.2 Hz), 5.92 (1H, s), 5.35 (2H, s), 5.11 (2H, s), 2.48 (3H, s). LC−MS 472.2 (M + H)$^+$.

4-[(Benzyloxy)methyl]-2-(2-chlorophenyl)-5-(pyrazin-2-ylmethyl)-1*H*-pyrazolo[4,3-*c*]pyridine-3,6(2*H*,5*H*)-dione (88). Isolated as a yellow solid. Mp 86−87 °C (HCl salt). ^{1}H NMR (400 MHz, DMSO-*d*$_6$) δ 8.57 (1H, s), 8.44 (2H, m), 7.65−7.58 (2H, m), 7.48− 7.46 (2H, m), 7.21−7.20 (3H, m), 7.12−7.10 (2H, m), 5.80 (1H, s), 5.48 (2H, s), 5.18 (2H, s), 4.49 (2H, s). LC−MS 474.1 (M + H)$^+$.

4-{[(2-Chlorobenzyl)oxy]methyl}-2-(2-chlorophenyl)-5-methyl-1*H*-pyrazolo[4,3-*c*]pyridine-3,6(2*H*,5*H*)-dione (89). Isolated as a yellow solid (15% yield). ^{1}H NMR (400 MHz, DMSO-*d*$_6$) δ 10.76 (1H, bs), 7.68−7.64 (1H, m), 7.60−7.57 (1H, m), 7.52−7.49 (3H, m), 7.45−7.43.39 (1H, m), 7.35−7.32 (2H, m), 5.82 (1H, s), 5.23 (2H, s), 4.67 (2H, s), 3.56 (3H, s). LC−MS 431.4 (M + H)$^+$.

2-(2-Chlorophenyl)-4-[(4-fluorophenoxy)methyl]-5-methyl-1*H*-pyrazolo[4,3-*c*]pyridine-3,6(2*H*,5*H*)-dione (90). Isolated as a yellow solid. Mp 129−130 °C (parent). ^{1}H NMR (400 MHz, DMSO-*d*$_6$) δ 10.85 (1H, bs), 7.64−7.55 (2H, m), 7.48−7.45 (2H, m), 7.12− 7.09 (4H, m), 5.84 (1H, s), 5.68 (1H, s), 3.55 (3H, s). LC−MS 400.0 (M + H)$^+$.

General Procedure D for the Synthesis of Compounds of Type 40. Starting from the appropriate pyrazolone **28** whose synthesis has been already described (pyrazolone method B), the following molecules were generated.

Step 1: Synthesis of α-Chloroketone Derivative of Type 37. A stirred mixture of the appropriate pyrazolone **28** (2.35 mmol) in acetonitrile (10 mL) was treated with 2-chloro-1,1,1-triethoxyethane (1.34 mL, 7.05 mmol) and glacial acetic acid (27 μL, 0.47 mmol) under N$_2$. The reaction mixture was heated to 70 °C and monitored by LC−MS until disappearance of starting material. The evaporation of the solvent until dryness by rotoevaporation at 45 °C allowed the reaction to go to completion. The crude dark oil was used in the following step without further purification.

Step 2: Synthesis of Enamine of Type 38. Compound from step 1 (2.25 mmol) was dissolved in acetonitrile (10 mL), and the appropriate amine (2.03 mmol) was added at room temperature under N$_2$. The reaction was monitored by UPLC−MS showing the disappearance of the starting material after only 10 min. The solvent was evaporated, and the crude product was used in the following step without further purification.

Step 3: Chloride Displacement. Compound from step 2 (2.25 mmol) was dissolved in acetonitrile (10 mL), and the appropriate amine (2.03 mmol) followed by DIPEA (0.392 mL, 2.25 mmol) was added at room temperature under N$_2$. The mixture was warmed to 50 °C until the disappearance of starting material. The solvent was evaporated, and the crude mixture was partitioned between ethyl acetate and an aqueous solution of saturated sodium bicarbonate. The combined organic layers were dried over Na$_2$SO$_4$ and concentrated in vacuo. The crude product was used in the following step without further manipulation or purified by silica plug.

Step 4: Cyclization. The enamine from step 3 (1.4 mmol) was treated with a freshly prepared solution of MeONa in MeOH (2 M, 20 mL). The solution was stirred at room temperature until disappearance of the starting enamine (0.5−2 h). The reaction mixture was concentrated in vacuo to evaporate MeOH, and the crude was dissolved in ethyl acetate (80 mL) and extracted with water (3 × 30 mL). The combined aqueous layers were acidified to pH 6 and extracted with ethyl acetate (3 × 30 mL). Then combined organic layers were dried over Na$_2$SO$_4$. The crude mixture was purified by silica chromatography or reverse phase chromatography to afford the desired product.

Following the described general procedure D, using the appropriate hydrazines and primary and secondary amines, compounds **81**, **83**, **85**, and **87** were obtained with 15−30% overall yield.

4-{[Benzyl(methyl)amino]methyl}-2-(2-chloro-4-fluorophenyl)-5-(3-methoxypropyl)-1*H*-pyrazolo[4,3-*c*]pyridine-3,6(2*H*,5*H*)-dione (81). Isolated as a yellow solid (93% HPLC purity). ^{1}H NMR (400 MHz, DMSO-*d*$_6$) δ 10.62 (1H, bs), 7.68 (1H, dd, *J* = 7.0 Hz, *J* = 2.2 Hz), 7.64 (1H, dd, *J* = 7.2 Hz, *J* = 4.8 Hz), 7.33−7.24 (6H, m), 5.72 (1H, s), 4.29 (2H, t, *J* = 6.2 Hz), 4.13 (2H, m), 3.60 (2H, s), 3.23 (3H, s), 2.14 (3H, s), 1.86−1.81 (2H, m). LC−MS 486.5 (M + H)$^+$.

2-(2-Chloro-4-fluorophenyl)-5-(2-pyridin-2-ylethyl)-4-(pyrrolidin-1-ylmethyl)-1*H***-pyrazolo[4,3-*c*]pyridine-3,6(2*H*,5*H*)-dione (83).** Isolated as a beige solid. Mp 163−164 °C (2HCl salt). ^{1}H NMR (400 MHz, DMSO-d_6) δ 8.8 (1H, d, J = 6.0 Hz), 8.56 (1H, t, J = 8.0 Hz), 8.07 (1H, d, J = 8.0 Hz), 7.99 (1H, t, J = 6.8 Hz), 7.70 (1H, dd, J = 8.8 Hz, J = 5.6 Hz), 7.53 (1H, dd, J = 8.4 Hz, J = 2.8 Hz), 7.32 (1H, td, J = 8.8 Hz, J = 2.8 Hz), 6.10 (1H, s), 5.35 (2H, s), 4.78 (2H, t, J = 7.2 Hz), 3.76−3.56 (4H, m), 3.65 (2H, t, J = 7.2 Hz), 2.25−2.10 (4H, m). LC−MS 468.1 (M + H)$^+$.

2-(2-Chlorophenyl)-4-{[4-(3-methoxyphenyl)piperazin-1-yl]methyl}-5-methyl-1*H***-pyrazolo[4,3-*c*]pyridine-3,6(2*H*,5*H*)-dione (85).** Isolated as a yellow solid. ^{1}H NMR (400 MHz, DMSO-d_6) δ 7.67−7.61 (2H, m), 7.51−7.48 (2H, m), 7.15 (1H, t, J = 8.2 Hz), 6.65−6.50 (2H, m), 6.50−7.40 (1H, m), 5.92 (1H, s), 3.70−3.3 (14H, m). LC−MS 480.1 (M + H)$^+$.

2-(2-Chlorophenyl)-5-[(1-methyl-1*H***-pyrazol-3-yl)methyl]-4-{[methyl(pyridin-3-ylmethyl)amino]methyl}-1***H***-pyrazolo[4,3-*c*]pyridine-3,6(2*H*,5*H*)-dione (87).** Isolated as a yellow solid. ^{1}H NMR (400 MHz, DMSO-d_6) δ 10.67 (1H, bs), 8.44 (1H, d, J = 1.6 Hz), 8.42 (1H, dd, J = 3.6 Hz, J = 1.2 Hz), 7.68−7.62 (2H, m), 7.60−7.55 (2H, m), 7.48 (2H, dd, J = 4.8 Hz, J = 2.8 Hz), 7.29 (1H, dd, J = 6.0 Hz, J = 3.6 Hz), 6.05 (1H, d, J = 1.6 Hz), 5.68 (1H, s), 5.55 (2H, s), 4.31−4.24 (2H, m), 3.73 (3H, s), 2.22 (3H, s). LC−MS 491.2 (M + H)$^+$.

Biological Assays. Plasmid Construction. Human Nox1 (NM_007052.4) cDNA was cloned into the pcDNA5/TO (Invitrogen). Human p22 (NM_000101.2) was cloned into pcDNA3.1/Zeo (+) (Invitrogen), and human NOXA1 (AY255769.1) and human NOXO1 (AB097667) were cloned into the bicistronic pVITRO1-neo-mcs plasmid (Invivogen).

Cell Culture and Stable Transfected Cell Line Generation. T-REx-CHO cells (Invitrogen) were cultured in Ham's F12 containing 4.5 g/L glucose supplemented with 10% fetal calf serum, 2 mM glutamine, penicillin (100 U/mL), streptomycin (100 μg/mL), and blasticidin (5 μg/mL). Cells stably expressing functional human Nox1 (hNOX1 T-REx-CHO) were obtained by co-transfecting T-REx-CHO with human NOX1, human p22, human NOXA1, and human NOXO1 using the FuGENE 6 method (Roche, 11988387).

T-REx-293 cell line expressing hNOX4 (hNOX4 T-REx-293) was a gift from the Department of Immunology and Pathology, University of Geneva, Switzerland.[55] hNOX4 T-REx-293 cells were cultured in DMEM containing 4.5 g/L glucose supplemented with 10% fetal calf serum, penicillin (100 U/mL), and streptomycin (100 μg/mL) at 37 °C in air with 5% CO_2. Human Nox1 and human Nox4 expression were induced with tetracycline (1 μg/mL) for 24 h prior to the membrane preparation.

Membrane Preparation. Membranes from human polymorphonuclear (PMN) cells (expressing high levels of Nox2) or from cells overexpressing Nox1 or Nox4 were prepared as previously described.[56] After resuspension in sonication buffer (11% sucrose, 120 mM NaCl, 1 mM EGTA in PBS, pH 7.4, for Nox4-expressing cells) or in relax buffer (10 mM Pipes, 3 mM NaCl, 3.5 mM MgCl$_2$, 0.1 M KCl, pH 7.4), cells were broken by sonication and centrifuged (200g, 10 min). The supernatant was layered onto a 17/40% (w/v) discontinuous sucrose gradient and centrifuged (150000g for 30 min). Membrane fractions were collected from the 17/40% interface and were stored at −80 °C. Protein concentration was determined with Bradford reagent.

ROS Production Measurement. Reactive oxygen species (ROS) production by membranes expressing human Nox1, human Nox2, or human Nox4 or by xanthine oxidase were measured using the Amplex Red (AR) method following a slightly modified version of the manufacturer's instruction manual (Invitrogen). Briefly, membranes expressing different Nox subunits or xanthine oxidase were incubated in PBS with Amplex Red, horseradish peroxidase (HRP), and appropriate cofactors. ROS production was induced by addition of NADPH to Nox expressing membranes or by addition of xanthine to xanthine oxidase. Nonspecific signal was measured in the absence of membranes or in the absence of agonist. Antagonist activity of compounds was measured in the presence of increasing concentrations ranging from 1 nM to 100 μM. After 20 min of incubation at 37 °C, ROS levels were measured using a BMG Labtech microplate reader.

Data Analysis. Data were analyzed using Prism (GraphPad Software Inc., San Diego, CA). K_i values were calculated using the Cheng−Prusoff equation and represent the average of at least three individual experiments performed in triplicate.

Oxidative Metabolism. Pooled human liver microsomes (pooled male and female) and pooled rat liver microsomes (male Sprague−Dawley rats) were used to screen the metabolic instability resulting from phase I oxidation. Microsomes (final concentration of 0.5 mg/mL), 0.1 M phosphate buffer, pH 7.4, and test compound (final substrate concentration of 0.5 μM; final DMSO concentration of 0.25%) were added to the assay plate and preincubated at 37 °C.

NADPH solution (final incubation concentration of 1 mM) was added to initiate the reaction. Each compound is incubated for 0, 5, 15, 30, and 45 min. The control (minus NADPH) was incubated for 45 min only. The reactions were stopped by the addition of 50 μL of methanol containing internal standard at the appropriate time points. The samples were centrifuged at 2500 rpm for 20 min at 4 °C to precipitate the protein. Samples were analyzed by LC/MS−MS. The percentage of compound disappearance and the in vitro intrinsic clearance were calculated according to the literature.[57]

Cytochrome P450 Inhibition. Six human recombinant cytochrome P450 isoenzymes (BD Gentest, Woburn, MA) were tested (CYP 1A2, CYP 2C8, CYP 2C9, CYP 2C19, CYP 2D6, and CYP 3A4). Test compound (0.1−25 μM) was incubated (final DMSO concentration of 0.3%) with specific species liver microsomes and NADPH in the presence of a cytochrome P450 isoform-specific probe substrate. For the CYP 2C8, CYP 2C9, CYP 2C19, CYP 2D6, and CYP 3A4 specific reactions, the metabolites were monitored by mass spectrometry. CYP 1A2 activity was monitored by measuring the formation of a fluorescent metabolite. A decrease in the formation of the metabolite compared to the vehicle control was used to calculate an IC$_{50}$ value.

Caco-2 Permeability. Caco-2 cells were obtained from American Type Culture Collection (Rockville, MD). The cells were seeded onto Millipore multiscreen Caco-2 plates at 1×10^5 cell/cm^2 and grown in Dulbecco's modified Eagle's medium, and media were changed every 2 or 3 days. Permeability studies were performed with the monolayers cultured for 20 days. On day 20, the monolayers were prepared by rinsing both basolateral and apical surfaces twice with HBSS at 37 °C. Prior to all experiments, the cell monolayer integrity was evaluated by trans epithelial electrical resistance; values greater than 800 Ω·cm^2 were used. Hank's balanced salt solution buffer was then removed from either the apical compartment (for apical to basolateral transport, A to B) or basolateral compartment (for basolateral to apical transport, B to A) side of the monolayer and replaced with test compound dosing solutions. The permeability studies were initiated by adding an appropriate volume of solution made by diluting 10 mM test compound in DMSO with HBSS pH 6.5 buffer to give a final test compound concentration of 10 μM (final DMSO concentration of 1%). The monolayers were then placed in an incubator at 37 °C. At the end of the incubation time (2 h), samples were taken from both the apical and basolateral compartments. Test and control compounds were quantified by LC−MS/MS cassette analysis using a five-point calibration with appropriate dilution of the samples. The permeability coefficient (P_{app}) was calculated according to the following equation: $P_{app} = (dQ/dt)/(C_0 A)$, where dQ/dt is the rate of permeation of the drug across the cell, C_0 is the donor compartment concentration at time zero, and A is the area of the cell monolayer. C_0 is obtained from analysis of donor and receiver compartments at the end of the incubation period.

In Vivo Pharmacokinetic Studies in Rat. These studies were conducted to estimate the plasma pharmacokinetic parameters

and the oral bioavailability of compounds in the male Sprague–Dawley rat. These studies were carried out using a parallel design using six male rats. Three animals in group 1 were given 5 mg/kg iv dose. Three animals in group 2 were given 10 mg/kg oral dose. Blood samples were collected from the carotid arterial cannula at various times up to 24 h following administration of compound. Plasma concentrations of compound were quantified by LC/MS/MS (LLOQ = 1.00 ng/mL). Noncompartmental methods were used for pharmacokinetic data analysis.

The vehicle used for per os administration was an aqueous solution of 0.5% CMC (carboxymethylcellulose) and 0.25% Tween 20. The vehicle used for iv injection was an aqueous solution of EDPW (10% EtOH, 10% DMA, 30% PG, and 50% water).

Supporting Information Available: Synthetic methods for compounds **18**, **19**, **41–45**, **46–48**; characterization data for compounds **8–11**, **13–17**, **50–52**, **55–62**, **64–66**, **69–77**, **80**, **86**, **91**; spectroscopic and analytical data for compounds **67**, **82**, **83**, **88**, **90**. This material is available free of charge via the Internet at http://pubs.acs.org.

References

(1) Galli, F.; Piroddi, M.; Annetti, C.; Aisa, C.; Floridi, E.; Floridi, A. Oxidative Stress and Reactive Oxygen Species. In *Cardiovascular Disorders in Hemodialysis*; Ronco, C., Brendolan, A., Levin, N. W., Eds.; Contributions to Nephrology, Vol. 149; Karger: Basel, Switzerland, 2005; pp 240–260.

(2) Reth, M. Hydrogen peroxide as second messenger in lymphocyte activation. *Nat. Immunol.* **2002**, *3*, 1129–1134.

(3) Bae, Y. S.; Kang, S. W.; Seo, M. S.; Baines, I. C.; Tekle, E.; Boon Chock, P.; Rhee, S. G. Epidermal growth factor (EGF)-induced generation of hydrogen peroxide. Role in EGF receptor-mediated tyrosine phosphorylation. *J. Biol. Chem.* **1997**, *272*, 217–221.

(4) Mahadev, K.; Zilbering, A.; Zhu, L.; Goldstein, B. J. Insulin-stimulated hydrogen peroxide reversibly inhibits protein–tyrosine phosphatase 1b in vivo and enhances the early insulin action cascade. *J. Biol. Chem.* **2001**, *276*, 21938–21942.

(5) Rhee, S. G.; Bae, Y. S.; Lee, S. R.; Kwon, J. Hydrogen peroxide: a key messenger that modulates protein phosphorylation through cysteine oxidation. *Sci. STKE* **2000**, *53*, 1–6.

(6) Bogdan, C. Nitric oxide and the immune response. *Nat. Immunol.* **2001**, *2*, 907–916.

(7) Finkel, T. Signal transduction by reactive oxygen species in non-phagocytic cell. *J. Leukocyte Biol.* **1999**, *65*, 337–340.

(8) Finkel, T. Reactive oxygen species and signal transduction. *IUBMB Life* **2001**, *52*, 3–6.

(9) Gamaley, I. A.; Klyubin, I. V. Roles of reactive oxygen species: signaling and regulation of cellular functions. *Int. Rev. Cytol.* **1999**, *188*, 203–255.

(10) Gulati, P.; Klöhn, P. C; Krug, H.; Göttlicher, M.; Markova, B.; Böhmer, F. D.; Herrlich, P. Redox regulation in mammalian signal transduction. *IUBMB Life* **2001**, *52*, 25–28.

(11) Dröge, W. Free radicals in the physiological control of cell function. *Physiol. Rev.* **2002**, *82*, 47–95.

(12) Quinn, M. T.; Ammons, M. C. B.; Deleo, F. R. The expanding role of NADPH oxidases in health and disease: no longer just agents of death and destruction. *Clin. Sci.* **2006**, *111*, 1–20.

(13) Cave, A. C.; Brewer, A. C.; Narayanapanicker, A.; Ray, R.; Grieve, D. J.; Walker, S.; Shah, A. M. NADPH oxidases in cardiovascular health and disease. *Antioxid. Redox Signaling* **2006**, *8*, 691–728.

(14) Bedard, K.; Krause, K. H. The Nox family of ROS-generating NADPH oxidases: physiology and pathophysiology. *Physiol. Rev.* **2007**, *87*, 245–313.

(15) Hordijk, P. L. Regulation of NADPH oxidase: the role of Rac proteins. *Circ. Res.* **2006**, *98*, 453–462.

(16) Cheng, G.; Cao, Z.; Xu, X.; Van Meir, E. G.; Lambeth, J. D. Homologs of gp91phox: cloning and tissue expression of Nox3, Nox4, and Nox5. *Gene* **2001**, *269*, 131–140.

(17) Guzik, T. J.; Harrison, F. G. Vascular NADPH oxidases as drug targets for novel antioxidant strategies. *Drug Discovery Today* **2006**, *11*, 524–533.

(18) Lambeth, J. D.; Krause, K. H.; Clark, R. A. NOX enzymes as novel targets for drug development. *Semin. Immunopathol.* **2008**, *30*, 339–363.

(19) Hecker, L.; Vittal, R.; Jones, T.; Jagirdar, R.; Luckhardt, T. R.; Horowitz, J. C.; Pennathur, S.; Martinez, F. J.; Thannickal, V. J. NADPH oxidase-4 mediates myofibroblast activation and fibrogenic responses to lung injury. *Nat. Med.* **2009**, *15*, 1077–1081.

(20) Li, S.; Tabar, S. S.; Malec, V.; Eul, B. G.; Klepetko, W.; Weissmann, N.; Grimminger, F.; Seeger, W.; Rose, F.; Hänze, J. NOX4 regulates ROS levels under normoxic and hypoxic conditions, triggers proliferation, and inhibits apoptosis in pulmonary artery adventitial fibroblasts. *Antioxid. Redox Signaling* **2008**, *10*, 1687–1697.

(21) Sanders, K. A.; Hoidal, J. R. The NOX on pulmonary hypertension. *Circ. Res.* **2007**, *101*, 224–226.

(22) Tojo, A.; Asaba, K.; Onozato, M. L. Suppressing renal NADPH oxidase to treat diabetic nephropathy. *Expert Opin. Ther. Targets* **2007**, *11*, 1011–1018.

(23) Matsushima, S.; Kinugawa, S.; Yokota, T.; Inoue, N.; Ohta, Y.; Hamaguchi, S; Tsutsui, H. Increased myocardial NAD(P)H oxidase-derived superoxide causes the exacerbation of postinfarct heart failure in type 2 diabetes. *Am. J. Physiol.: Heart Circ. Physiol.* **2009**, *297*, 409–416.

(24) Gao, L.; Mann, G. E. Vascular NADPH oxidase activation in diabetes: a double-edged sword in redox signalling. *Cardiovasc. Res.* **2009**, *82*, 9–20.

(25) Juhasz, A.; Ge, Y.; Markel, S.; Chiu, A.; Matsumoto, L.; Van Balgooy, J.; Roy, K.; Doroshow, J. H. Expression of NADPH oxidase homologues and accessory genes in human cancer cell lines, tumours and adjacent normal tissues. *Free Radical Res.* **2009**, *43*, 523–532.

(26) Maranchie, J. K.; Zhan, Y. Nox4 is critical for hypoxia-inducible factor 2-A transcriptional activity in von Hippel–Lindau-deficient renal cell carcinoma. *Cancer Res.* **2005**, *65*, 9190–9193.

(27) Block, K.; Gorin, Y.; Hoover, P.; Williams, P.; Chelmicki, T.; Clark, R. A.; Yoneda, T.; Abboud, H. E. NAD(P)H oxidases regulate HIF-2alpha protein expression. *J. Biol. Chem.* **2007**, *282*, 8019–8026.

(28) Gill, P. S.; Wilcox, C. S. NADPH oxidases in the kidney. *Antioxid. Redox Signaling* **2006**, *8*, 1597–1607.

(29) Chabrashvili, T.; Tojo, A.; Onozato, M. L.; Kitiyakara, C.; Quinn, M. T.; Fujita, T.; Welch, W. J.; Wilcox, C. S. Expression and cellular localization of classic NADPH oxidase subunits in the spontaneously hypertensive rat kidney. *Hypertension* **2002**, *39*, 269–274.

(30) Shiose, A.; Kuroda, J.; Tsuruya, K.; Hirai, M.; Hirakata, H.; Naito, S.; Hattori, M.; Sakaki, Y; Sumimoto, H. A novel superoxide-producing NAD(P)H oxidase in kidney. *J. Biol. Chem.* **2001**, *276*, 1417–1423.

(31) Nisbet, R. E.; Graves, A. S.; Kleinhenz, D. J.; Rupnow, H. L.; Reed, A. L.; Fan, T. M.; Mitchell, P. O.; Sutliff, R. L.; Hart, C. M. The role of NADPH oxidase in chronic intermittent hypoxia-induced pulmonary hypertension in mice. *Am. J. Respir. Cell Mol. Biol.* **2009**, *40*, 601–609.

(32) Van der Vliet, A. NADPH oxidases in lung biology and pathology: host defense enzymes, and more. *Free Radical Biol. Med.* **2008**, *44*, 938–955.

(33) Raghu, G.; Weycker, D.; Edelsberg, J.; Bradford, W. Z.; Oster, G. Incidence and prevalence of idiopathic pulmonary fibrosis. *Am. J. Respir. Crit. Care Med.* **2006**, *174*, 810–816.

(34) Psathakis, K.; Mermigkis, D.; Papatheodorou, G.; Loukides, S.; Panagou, P.; Polychronopoulos, V.; Siafakas, N. M.; Bouros, D. Exhaled markers of oxidative stress in idiopathic pulmonary fibrosis. *Eur. J. Clin. Invest.* **2006**, *36*, 362–367.

(35) Aldieri, E.; Riganti, C.; Polimeni, M.; Gazzano, E.; Lussiana, C.; Campia, I.; Ghigo, D. Classical inhibitors of Nox NADPH oxidases are not specific. *Curr. Drug Metab.* **2008**, *9*, 686–696.

(36) Tazzeo, T.; Worek, F.; Janssen, L. J. The NADPH oxidase inhibitor diphenyleneiodonium is also a potent inhibitor of cholinesterases and the internal Ca^{2+} pump. *Br. J. Pharmacol.* **2009**, *158*, 790–796.

(37) Yu, J.; Weiwer, M; Linhardt, R. J.; Dordick, J. S. The role of the methoxyphenol apocynine, a vascular NADPH oxidase inhibitor, as a chemopreventative agent in the potential treatment of cardiovascular diseases. *Curr. Vasc. Pharmacol.* **2008**, *6*, 204–217.

(38) Ximenes, V. F.; Kanegae, M. P. P; Rissato, S. R.; Galhiane, M. R. The oxidation of apocynin catalyzed by myeloperoxidase: proposal for NADPH oxidase inhibition. *Arch. Biochem. Biophys.* **2006**, *2*, 134–141.

(39) Heumüller, S.; Wind, S.; Barbosa-Sicard, E.; Schmidt, H.; Busse, R.; Schröder, K.; Brandes, R. P. Apocynin is not an inhibitor of vascular NADPH oxidases but an antioxidant. *Hypertension* **2008**, *51*, 211–217.

(40) Williams, H. C.; Griendling, K. K. NADPH oxidase inhibitors: new antihypertensive agents? *J. Cardiovasc. Pharmacol.* **2007**, *50*, 9–16.

(41) Jaquet, V; Scapozza, L.; Clark, R. A.; Krause, K. H.; Lambeth, J. D. Small-molecule NOX inhibitors: ROS-generating NADPH oxidases as therapeutic targets. *Antioxid. Redox Signaling* **2009**, *10*, 1–18.

(42) Genkyotex unpublished internal data.

(43) Seno, K.; Nishi, K.; Matsuo, Y.; Fujishita, T. Pyrazolo (1,5-A) Pyrimidine Derivative and NADPH Oxidase Inhibitor Containing the Same. US2006/0089362, 2006; Shionigi.

(44) Tegtmeier, F.; Walter, U.; Schinzel, R.; Wingler, K.; Scheurer, P.; Schmidt, H. Compounds Containing a N-Heteroaryl Moiety Linked to Fused Ring Moieties for the Inhibition of NADPH Oxidases and Platelet Activation. WO2005/111041, 2005; Vasopharm GMBH.

(45) Cayatte, A. J.; Rupin, A.; Oliver-Krasinski, J.; Maitland, K.; Sansilvestri-Morel, P.; Boussard, M.; Wierzbicki, M.; Verbeuren, T. J.; Cohen, R. A. S17834, a New Inhibitor of Cell Adhesion and Atherosclerosis That Targets NADPH Oxidase. *Arterioscler., Thromb., Vasc. Biol.* **2001**, *21*, 1577–1584.

(46) Bhandarkar, S.; Jaconi, M.; Fried, L. E.; Bonner, M. Y.; Lefkove, B.; Govindarajan, B.; Perry, B. N.; Parhar, R.; Mackelfresh, J.; Sohn, A.; Stouffs, M.; Knaus, U.; Yancopoulos, G.; Reiss, Y.; Benest, A. V.; Augustin, H. G.; Arbiser, J. L. Fulvene-5 potently inhibits NADPH oxidase 4 and blocks the growth of endothelial tumors in mice. *J. Clin. Invest.* **2009**, *119*, 2359–2365.

(47) Steffen, Y.; Gruber, C.; Schewe, T.; Sies, H. Mono-O-methylated flavanols and other flavonoids as inhibitors of endothelial NADPH oxidase. *Arch. Biochem. Biophys.* **2008**, *469*, 209–219.

(48) Bevk, D.; Jakse, R.; Svete, J.; Golobic, A.; Golic, L.; Stanovnik, B. Transformations of alkyl (5-oxo-1-phenyl-4,5-dihydro-1*H*-pyrazol-3-yl)acetates into 5-heteroaryl-3-oxo-2-phenyl-3,5-dihydro-2*H*-pyrazolo[4,3-*c*]pyridine-7-carboxylates. *Heterocycles* **2003**, *61*, 197–223.

(49) Bieringer, S.; Holzer, W. 4-Acyl-5-hydroxy-1-phenyl-3-trifluoromethylpyrazoles: synthesis and NMR spectral investigations. *Heterocycles* **2006**, *68*, 1825–1836.

(50) Belmar, J.; Pérez, F. R.; Alderete, J.; Zuniga, C. Synthesis and tautomeric studies of enamines from 1-(*n*-hexyl)-3-methyl-2-pyrazolin-5-one. *J. Braz. Chem. Soc.* **2005**, *16*, 179–189.

(51) Balogh, M.; Hermecz, I.; Simon, K.; Pusztay, L. Studies on naphthyridines. Part 2. Synthesis of 4-substituted and 6-substituted 1,6-naphthyridin-5(6*H*)-ones. *J. Heterocycl. Chem.* **1989**, *26*, 1755–1769.

(52) Vilar, J.; Quintela, J. M.; Peinador, C.; Veiga, C.; Ojea, V. Synthesis of 1,7,10-anthyridine derivatives. *Heterocycles* **1993**, *36*, 2697–2705.

(53) Jensen, B. S. The synthesis of 1-phenyl-3-methyl-4-acyl-pyrazolones-5. *Acta Chem. Scand.* **1959**, *13*, 1668–1670.

(54) Batezila, G.; Holzer, W. Synthesis of 1,7,10-anthyridine derivatives. *Molbank* **2010**, *36*, M661.

(55) Serrander, L.; Cartier, L.; Bedard, K.; Banfi, B.; Lardy, B.; Plastre, O.; Sienkiewicz, A.; Fórró, L.; Schlegel, W.; Krause, K. H. NOX4 activity is determined by mRNA levels and reveals a unique pattern of ROS generation. *Biochem. J.* **2007**, *406*, 105–114.

(56) Palicz, A.; Foubert, T. R.; Jesaitis, A. J.; Marodi, L.; McPhail, L. C. Phosphatidic acid and diacylglycerol directly activate NADPH oxidase by interacting with enzyme components. *J. Biol. Chem.* **2001**, *76*, 3090–3097.

(57) Lave, T. H.; Dupin, S.; Schmitt, C.; Chou, R. C.; Jack, D.; Coassolo, P. H. Integration of in vitro data into allometric scaling to predict hepatic metabolic clearance in man: application to 10 extensively metabolized drugs. *J. Pharm. Sci.* **1997**, *86*, 584–590.

(58) Page, P.; Orchard, M.; Laleu, B.; Gaggini, F. Preparation of Pyrazolopyridine Derivatives as NADPH Oxidase Inhibitors. WO2010/035220, WO2010/035221, WO2010/035219, WO2010/035217, 2010; Genkyotex. Page, P.; Orchard, M.; Fioraso-Cartier, L.; Mottironi, B. Preparation of Pyrazolopyridine Derivatives as NADPH Oxidase Inhibitors. WO2008/113856, 2008; Genkyotex.